

Aggregation Analysis of the Microtubule Binding Domain in Tau Protein by Spectroscopic Methods

Tian-Ming Yao^{*1}, Koji Tomoo^{*1}, Toshimasa Ishida¹, Hiroshi Hasegawa², Masahiro Sasaki² and Taizo Taniguchi^{2,3}

¹Osaka University of Pharmaceutical Sciences, 4-20-1 Nasahara, Takatsuki, Osaka 569-1094; ²Behavioral and Medical Sciences Research Consortium, 2-5-7 Tamachi, Akashi, Hyogo 673-0025; and ³Biosignal Research Center, Kobe University, 1-1 Rokkodai-cho, Nada, Kobe 657-8501

Received March 4, 2003; accepted May 2, 2003

The microtubule-associated protein tau is a highly soluble protein that shows hardly any tendency to assemble under physiological conditions. In the brains of Alzheimer's disease (AD) patients, however, tau dissociates from the axonal microtubule and abnormally aggregates to form paired helical filaments (PHFs). One of the priorities in Alzheimer research is to clarify the mechanism of PHF formation. In recent years, several factors regulating tau assembly have come to light, yet some important questions remain to be answered. In this work, the His-tagged gene constructs of the four-repeat microtubule binding domain (4RMBD) in tau protein and its three mutants, 4RMBD S305N, N279K, and P301L, were expressed in *E. coli* and purified. Gel filtration chromatography and dynamic light scattering measurement yielded a Stokes radius of 3.1 nm, indicating that the His-tagged 4RMBD normally exists in buffer solution in a dimer state, which is formed by non-covalent intermolecular interactions. This non-covalent dimer can further polymerize to form filaments in the presence of polyanions such as heparin. The kinetics of the *in vitro* aggregation was monitored by thioflavine S dye fluorescence and CD measurements. The aggregation of 4RMBD was suggested to be a nucleation-dependent process, where the non-covalent dimer acts as an effective structural unit. The aggregation rate was strongly affected by the point mutation. Among the 4RMBD mutants, the rate of S305N was exceptionally fast, whereas N279K was the slowest, even slower than the wild-type. The aggregations were optimal in a weakly reducing environment for all the mutants and the wild type. However, the aggregations were affected differently by buffer pH, depending on the 4RMBD mutation.

Key words: aggregation, tau protein, spectroscopic analysis.

Abbreviations: AD, Alzheimer's disease; CD, circular dichroism; DLS, dynamic light scattering; DTT, dithiothreitol; FPLC, fast protein liquid chromatography; FTDP-17, Frontotemporal Dementia with Parkinsonism linked to Chromosome 17; MES, 2-(*N*-morpholino) ethanesulfonic acid; NFTs, neurofibrillary tangles; PBS, Phosphate-buffered saline; PHFs, paired helical filaments; PIPES, piperazine-*N,N'*-bis(2-ethanesulfonic acid); 4RMBD, tau construct with four-repeat microtubule binding domain; SDS-PAGE, sodium dodecylsulfate polyacrylamide gel electrophoresis; ThS, thioflavine-S.

Alzheimer's disease (AD) is the most common cause of dementia in the elderly population. AD is accompanied by a number of structural and metabolic alterations in the brain, and is characterized by two histopathological hallmarks, extracellular deposits of β -amyloid in neuritic plaques and intracellular neurofibrillary tangles (NFTs) (1). The latter are composed of bundles of paired helical filaments (PHFs), the abnormal aggregation of tau protein. Tau is one of the main, though not exclusive, neuronal microtubule-associated proteins. The most important function of tau is the stabilization of axonal microtubules (2). It is a highly soluble protein and shows hardly any tendency to assemble under physiological conditions. In the brains of AD patients, however, tau dissociates from its natural partner, the microtubule, and aggregates to

form insoluble fibers (3). The principle of these tau pathologies remains elusive.

In adult human brain, multiple tau isoforms are expressed from a single gene comprising 15 exons. By alternative splicing of exons 2, 3 and 10, six major tau isoforms consisting of 352 to 441 amino acids are produced (4). Recently, a group of frontotemporal dementias, now termed FTDP-17, was found to be related to mutations in tau (5). At present, eight mutants (G272V, N279K, Δ K280, P301L, P301S, S305N, V337M, and R406W) of tau protein have been identified in FTDP-17 (4), and most of them, *i.e.*, N279K, Δ K280, P301L, P301S, and S305N, cluster in the four-repeat microtubule binding domain (4RMBD). Besides leading to a reduced ability of tau to interact with microtubules, or to increase alternative mRNA splicing of exon 10, missense and deletion mutants in tau may have an additional effect, the stimulation of filament assembly. Phosphorylation is believed to be another factor that negatively modulates

^{*}To whom correspondence should be addressed. Tel/Fax: +81-726-90-1068, E-mail: yao@gly.oups.ac.jp; tomoo@gly.oups.ac.jp

the function of microtubule stabilization (6). Hyperphosphorylation is an invariant feature of the filamentous tau deposits in neurodegenerative diseases (7).

One of the priorities in Alzheimer research is to clarify the mechanism of PHF formation. However, the progress of such investigations using model systems such as transfected cells or transgenic mice has been relatively slow (8), and our knowledge on tau aggregation stems largely from *in vitro* data.

Tau has resisted all efforts of crystallization; therefore, most of the structural information so far was obtained by spectral methods. These data indicate a natively unfolded conformation with very little secondary structure (9, 10). This loose and open structure may explain why tau survives in the presence of heat, denaturants or acid without losing its biological function. In recent years, several factors regulating tau assembly have emerged (11): (i) Polyanion stimulates assembly by compensating for the positive charge (12, 13). (ii) A three- or four-repeat microtubule binding domain in tau aggregates more readily than full-length tau (14). (iii) Some but not all types of tau mutations lead to accelerated filament formation (15–18). (iv) The aggregation reaction is a nucleation-dependent process (19). (v) The aggregation is strongly promoted by covalent-bonded dimerization through Cys322 of tau (20).

Advances by *in vitro* experimental approaches have opened the way towards a systematic study of the assembly mechanism of tau protein. But still, some important questions remain to be answered. For example, is tau aggregation based on β -sheet formation or some other structure? What is the building block of the filament? How does buffer pH affect aggregation? Which environmental condition, oxidizing or reducing, promotes aggregation? More detailed inspections should be conducted.

With these in mind, we have performed a study on the kinetics of tau aggregation. His tagged gene constructs of 4RMBD in tau protein and its three mutants, 4RMBD N279K, P301L and S305N (Fig. 1), were expressed and purified. The aggregation rates of 4RMBDs *in vitro* were monitored by the thioflavine S (ThS) dye fluorescence method and CD measurement. Several factors regulating the aggregation reaction are discussed based on these data.

MATERIALS AND METHODS

Chemicals and Recombinant Proteins—Heparin [average molecular weight (MW), 6000], bovine albumin, ovalbumin, lysozyme, and ThS were obtained from Sigma. A cDNA (clone T9) encoding human brain tau was kindly provided by Professor H. Mori (Osaka City Univ.). Wild-type 4RMBD constructs (Fig. 1) were prepared by PCR amplification using clone T9 as the template, according to a previous paper (6). The N279K, P301L, and S305N mutants of 4RMBD were prepared using a Quick-Change Site-directed Mutagenesis Kit (Stratagene). After their sequences were confirmed, they were subcloned into a pET23-NHis vector, constructed from the pET-23d vector (Novagen) by adding 8 amino acids (MHHHHHHM, where M and H are methionine and histidine residues, respectively) to the N-terminus of the 4RMBD as a His-tag. His-tagged wild-type and mutant 4RMBDs were expressed in *Escherichia coli* transformed by these vec-

tors, according to the instructions of the manufacturer (Novagen). Bacteria pellets were re-suspended in lysis buffer (50 mM Tris-HCl pH 7.5, 50 mM NaCl, containing protease inhibitor) and sonicated. The supernatants were then purified by the following three steps: (i) Cation-exchange FPLC. Column: HiPrep 16/10 SP XL (Amersham Biosciences). Eluting buffer: 50 mM Tris-HCl, pH7.5, 1 mM DTT with a gradient of NaCl. (ii) Nickel-chelating Sepharose (Amersham Biosciences, gravity flow column), step-washed with imidazol in 50 mM Tris-HCl, pH7.5, buffer, containing 0.5 M NaCl. (iii) Gel filtration FPLC. Column: Superdex 75 HR 10/30 (Amersham Biosciences). Eluting buffer: 50 mM Tris-HCl, pH 7.5, 150 mM NaCl. The purity after each purification step was checked by SDS-PAGE. Protein concentrations were determined by UV absorption at 280 nm. A schematic diagram of the full-length tau, its His-tagged four-repeat domain (His 4RMBD), and related MBD constructs are shown in Fig. 1, where the numbering of amino acid residues corresponds to the longest isoform of human tau of 441 residues.

Dynamic Light Scattering (DLS) Analysis—All measurements were performed at 20°C using a DynaPro-801 molecular sizing instrument (Protein Solutions, Charlottesville, VA). The AutoPro software package was used for all data analyses. In the experiment, a protein solution in a 7 μ l flow cell was illuminated by a 25 mW, 780 nm solid-state laser, and the intensity of light scattered at an angle of 90° was measured at intervals of approximately 4 μ s by a solid-state avalanche photodiode. Using an autocorrelation function, the translational diffusion coefficient ($D\tau$) of the sample particles in solution was evaluated by measuring the fluctuations in the intensity of the scattered light. The hydrodynamic radius (R_H) of the sample particle was derived from $D\tau$ using the Stokes-Einstein equation, $D\tau = k_b T / 6\pi\eta R_H$, where k_b is the Boltzmann constant, T is absolute temperature, and η is solvent viscosity. The mass of the sample particles was estimated from R_H assuming that the particles are spherical and of standard density. Based on an attempt to fit the sizes of the sample particles to monomodal distribution (one particle size), the polydispersity, baseline, and sum-of-squares parameters give an indication of the homogeneity of the particle sizes in the sample.

Purified 4RMBDs were concentrated to 10 mg/ml in Millipore centrifugal filter devices. Protein samples of 300 μ l in volume were filtered through 0.1 μ m inorganic membranes (Whatman Anotop) before being placed in the DLS cuvette.

Molecular Size Estimation by Gel Filtration Chromatography—A HiLoad Superdex 75 16/60 (Amersham Biosciences) column was used for gel filtration chromatography. The elution buffer was 50 mM Tris-HCl (pH 7.5), containing 150 mM NaCl. The flow rate was controlled at 0.5 ml/min. Three protein samples with different molecular mass, BSA (66.4 kDa), ovalbumin (44.3 kDa), and lysozyme (14.3 kDa), were selected as the standards for column calibration. These were mixed and dissolved in 50 mM Tris-HCl buffer (pH 7.5) to a concentration of 0.1 mM for each protein component, and 1.0 ml of the standard protein solution was applied to the column. A calibration curve was thus obtained for the calculation of apparent MW from the elution volume. A sample solution (10

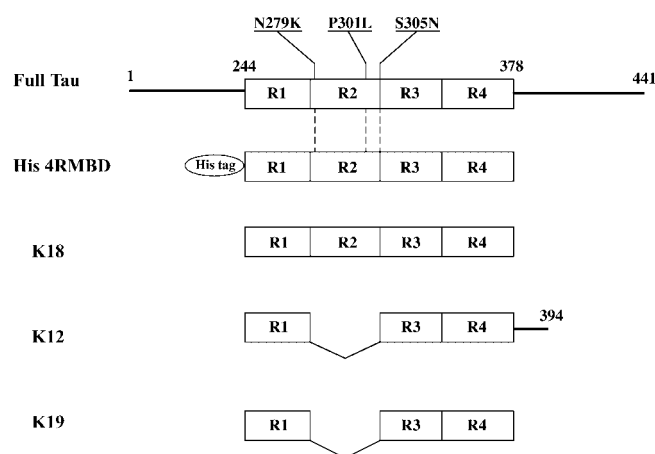


Fig. 1. **Schematic diagram of the full-length human tau protein (clone T9), His 4RMBD and related tau constructs.** The positions of the FTDP-17 mutations used in this work are indicated. The regions from the first to fourth MT-binding repeat are represented as R1 to R4. The numbering of the amino acid residues refers to the longest isoform of human tau (441 residues). From top to bottom: Full-length tau (the longest isoform in the human central nervous system, 441 residues), His 4RMBD (tau construct containing 4 pseudo-repeats with a His tag at the N-terminus). K18 (tau construct comprises 4 pseudo-repeats, R1–R4, ~31 residues each), K12 (tau construct comprises 3 pseudo-repeats and a short tail at the C-terminus, 121 residues), and K19 (tau construct comprises 3 pseudo-repeats, R1, R3, and R4)

mg/ml) of 4RMBDs was applied to the column under the same conditions.

Electron Microscopy—15 μ M 4RMBD tau was mixed with 3.8 μ M heparin in 50 mM Tris-HCl, pH 7.5, containing 1 mM DTT, and the solution was incubated at 37°C for 100 min. A 600-mesh copper grid was used for negative staining EM. A drop of the protein solution was placed on the grid along with a drop of 2% uranyl acetate. After 2 min, excess fluid was removed from the grid. Negative-staining electron microscopy was performed in an electron microscope (Hitachi H-600.) operated at 75 kV.

Monitoring 4RMBD Aggregation by Fluorescence Measurement—Wild-type and mutant 4RMBDs were adjusted to a concentration of 15 μ M using 50 mM Tris-HCl buffer (pH 7.5) containing 1 mM DTT and 10 μ M ThS dye. Aggregation was induced by adding heparin to the solution (final concentration 3.8 μ M), and mixing with a pipette prior to fluorescence measurement. A fluorescence time scan was obtained on a JASCO FP-770F instrument with a 2-mm quartz cell, with the temperature kept at 37°C by a circulating water bath. The kinetics of 4RMBD aggregation was analyzed by recording the time-dependent curve of fluorescence intensity with excitation at 440 nm and emission at 490 nm. The excitation and emission slit widths were set at 10 nm. Background fluorescence of the sample was subtracted when needed.

CD Spectra—15 μ M 4RMBD and 3.8 μ M heparin were mixed in 50 mM Tris-HCl buffer (pH 7.5) containing 1 mM DTT, and incubated at 37°C. Prior to recording the circular dichroism (CD) spectrum, the sample solution was diluted in 20 mM phosphate buffer (pH 6.8) to a concentration of 2 μ M protein and then transferred into a 2.0-mm-path-length quartz cell. Measurements were performed with a JASCO FP-720 spectropolarimeter coupled

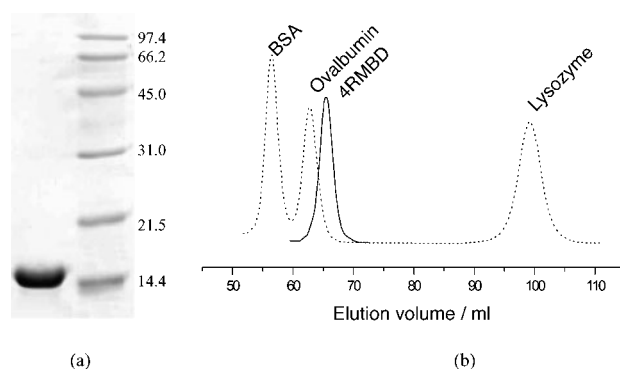


Fig. 2. (a) **SDS-PAGE of the 4RMBD wild type construct.** On the left is the band of the wild type 4RMBD. On the right are the molecular mass markers. (b) **Gel filtration FPLC for the estimation of the molecular size of the wild-type His 4RMBD.** Gel filtration was carried out on a Superdex 75 column, using 50 mM Tris-HCl (pH 7.5) containing 150 mM NaCl as the elution buffer at a flow rate of 0.5 ml/min. BSA (66.4 kDa), ovalbumin (44.3 kDa) and lysozyme (14.3 kDa) were used as the standard proteins for the estimation of molecular mass. The elution volumes are: 56.5 ml (BSA), 63.0 ml (ovalbumin), and 99.0 ml (lysozyme). The elution volume of 4RMBD is 66 ml, indicating a molecular mass of 43 kDa, corresponding to the hydrodynamic radius of ~3.0 nm.

with a data processor for summing up the signals. All the CD spectra were recorded over the wavelength range of 190–250 nm at 37°C under a flow of dry N_2 gas. The scan speed was 50 nm/min. For each spectrum the measurement was performed eight times and averaged.

RESULTS

Hydrodynamic Size of 4RMBD Constructs in Solution—SDS-PAGE revealed that the purity of the 4RMBD samples was very high, with a molecular mass corresponding to the protein band of ~14.5 kDa, consistent with the theoretical value of 4RMBD constructs (Fig. 2a). On the other hand, however, the retention time for gel filtration was much shorter than anticipated, probably due to the oligomerization of the protein in buffer solution. A detailed investigation of the oligomer state of 4RMBD in buffer solution was thus performed.

Systematic gel filtration chromatography was carried out to estimate the oligomer size of 4RMBD. In Fig. 2b, the elution volumes of standard proteins were 56.5 ml (BSA, 66.4 kDa), 63.0 ml (ovalbumin, 44.3 kDa), and 99.0 ml (lysozyme, 14.3 kDa), respectively, while the elution volume of wild-type 4RMBD was 66 ml. According to the relationship between elution volume and molecular mass of standard proteins (column's calibration curve), the apparent molecular mass of 4RMBDs was estimated at ~43 kDa, about three times the theoretical value. The elution volumes of the 4RMBD mutants, S305N, P301L, and N279K, were the same as that of wild-type, suggesting that the wild-type 4RMBD and its mutants probably exist in an oligomer state (named **S**, see below) under such buffer conditions.

To substantiate further the oligomer state of 4RMBD in buffer solution, DLS analyses were performed. The hydrodynamic radii (R_H) of 4RMBDs in buffer solution could be estimated from the variation of scattered light at

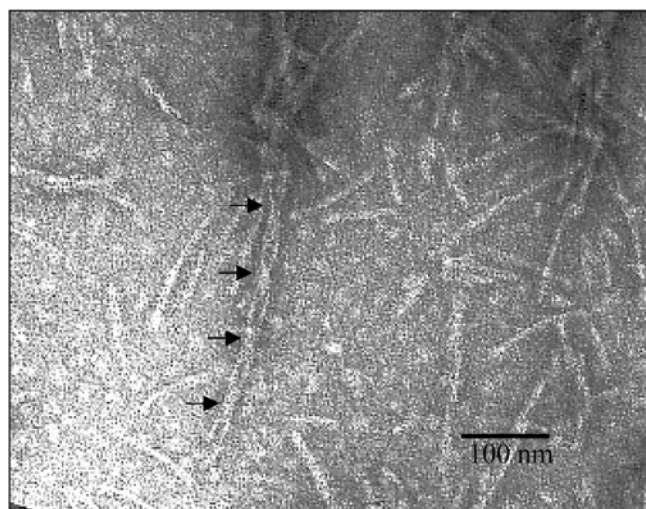


Fig. 3. **Electron micrograph of PHF of wild-type 4RMBD.** The sample was negatively stained with 2% uranyl acetate. Arrows indicate the typical PHF ultrastructure, the double-stranded twisted appearance with a cross-over repeat of ~80 nm.

90°. The DLS data are listed in Table 1. Again, this experiment showed that the average R_H of wild-type and mutant 4RMBDs are about 3.10 nm, corresponding to a hydrodynamic size of ~45 kDa.

Kinetic Analysis of the Filament Formation Reaction—Electron microscopy (EM) (Fig. 3) shows that the aggregated 4RMBD has a typical PHF ultrastructure, a double-stranded twisted appearance with a cross-over repeat of ~80 nm, which is similar to that of full-length tau protein (11). This implies that the PHF formation of tau protein can be monitored by its 4RMBD fragment.

It has been reported that thioflavine dyes such as ThS, which has been applied to staining NFTs in postmortem brain (21), can also be used to quantify PHF formation in solution in real time (22). We used this assay to monitor the kinetics and to examine factors influencing filament assembly.

The aggregation of wild-type 4RMBD at various concentrations was induced by heparin. The kinetics of aggregation was then monitored from the time dependence of the fluorescence intensity. As shown in Fig. 4a, the fluorescence intensity reached a maximum within 40

Table 1. **Dynamic light scattering measurements of wild-type and mutated 4RMBDs.**

Protein	Molecule R_H^a (nm)	Molecular mass (kDa)	Polydispersity (nm) ^b	SOS _{error} ^c
Wild	3.08	44.7	0.8	13.400
S305N	3.10	45.1	0.7	9.614
P301L	3.18	47.8	0.8	12.127
N270K	3.09	44.7	0.6	8.761

^aMean hydrodynamic radius derived from the measured translational diffusion coefficient using the Stokes-Einstein equation.

^bPolydispersity value, indicating the standard deviation of the distribution of particle size about the reported mean radius. ^cSum of squares measuring the closeness of fit between the experimental data and an autocorrelation function generated from the analysis results.

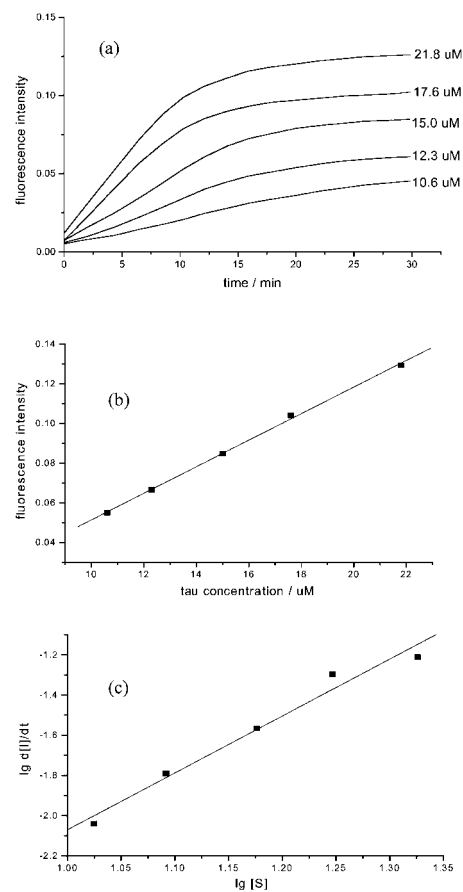
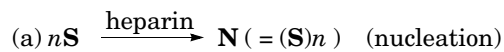


Fig. 4. **Kinetic analyses of the *in vitro* aggregation of wild-type 4RMBD.** The protein concentration was adjusted in range of 10.6 mM to 21.8 mM, using 50 mM Tris-HCl buffer (pH7.5) containing 1 mM DTT and 10 μ M ThS dye. Aggregation was induced by adding heparin to the solution (final concentration 3.8 μ M) and mixing with a pipette prior to fluorescence measurement. The kinetics of aggregation of the wild-type 4RMBD protein was observed from the fluorescence time scan. (a) Time dependence of the fluorescence intensity. (b) Calibration of maximum fluorescence intensity with MBD4s concentration. (c) Linear regression analysis of data $\log d[I]/dt$ versus $\log[S]$: $\log d[I]/dt = -4.90163 + 2.83079 \log[S]$, where $d[I]/dt$ is the maximum assembly rate obtained from the time dependence curve in (a), the slope in the initial 5 min.

min., with a half-time of about 5 min. A linear relationship between maximum fluorescence intensity and sample concentration (Fig. 4b) indicates that the fluorescence intensity is proportional to the amount of filaments formed in solution, $I = K[C]$, where I and C represent the intensity of ThS fluorescence and the filament concentration respectively, and K is a constant.

Gel filtration experiments and DLS analyses revealed that 4RMBD exists as oligomers (the subunit, named state **S**) in Tris-HCl buffer (pH 7.5). Hence, the whole process of filament formation can be regarded as a transition of the aggregation state, from the oligomer (subunit, state **S**), to the polymer (filament, state **F**), and the following two steps are possible:



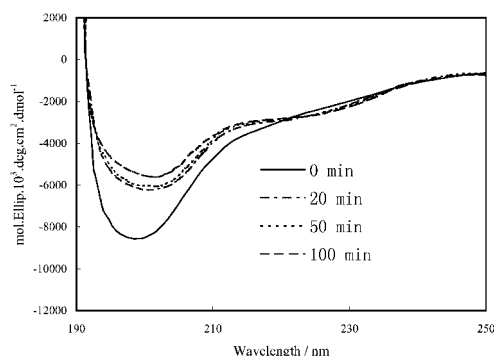


Fig. 5. **Change of the CD spectrum with the process of filament formation.** 4RMBD (15 μM) was mixed with heparin (3.8 μM) in 50 mM Tris-HCl buffer (pH 7.5) containing 1 mM DTT, and incubated at 37°C. After different incubation times, a small amount of solution was taken out and diluted (7 times) in 20 mM phosphate buffer (pH 6.8) for CD measurements.

where **N** represents a nucleus comprising n subunits **S**. Suppose that the elongation step can be ignored (this is reasonable, because few nuclei **N** exist in solution at the beginning of the spontaneous aggregation), then, the maximum rate of PHF formation at the beginning of the reaction should be determined by the nucleation step (a),

$$\frac{d[\mathbf{N}]}{dt} = k[\mathbf{S}]^n.$$

The increasing rate of fluorescence intensity should be

$$\begin{aligned} \frac{d[I]}{dt} &= K \frac{d[\mathbf{N}]}{dt} = Kk[\mathbf{S}]^n \\ \log \frac{d[I]}{dt} &= \log(Kk) + n \log[\mathbf{S}] \\ &= A + n \log[\mathbf{S}] \quad (A = \log(Kk)), \end{aligned}$$

where $d[I]/dt$ is obtained from the increasing slope of fluorescence intensity during the initial 5 min of each experiment (Fig. 4a). According to the above equation, a double log plot of $d[I]/dt$ vs. the concentration of sample **[S]** (oligomer) should give a straight line with a slope of n . Such a linear plot was indeed obtained (Fig. 4c). Using the linear fitting method, we calculated the slope $n = 2.83$ with a correlation coefficient of $r = 0.9874$. A good linear correlation supports our assumption that filament formation is a nucleation-controlled reaction. This result is consistent with the value reported in the literature (19), where aggregation was examined using dimeric tau K19 (linked by an intermolecular disulfide bond). The value $n = 2.83$ means that the nucleus consists of about three subunits **S**.

Filament Formation Alters the Random Coil Structure of 4RMBD—In order to investigate the possible conformational change that occurs during the process of PHF formation, we measured CD spectra, which are sensitive to the overall secondary structure of a protein (23). From the ThS fluorescence results, it is already clear that, although 4RMBD forms a filament structure at concentration of about 15 μM in Tris-HCl buffer (pH 7.5) in the presence of heparin, such aggregation does not proceed effectively, if the protein concentration is too low, or if the

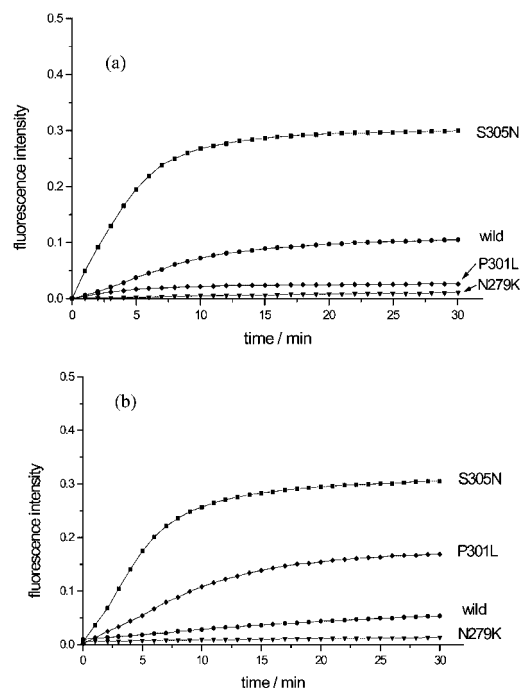


Fig. 6. **Aggregation of different 4RMBD mutants into filaments.** The protein was adjusted to a concentration of 15 μM using buffer solution containing 1 mM DTT and 10 μM ThS dye. Aggregation was induced by adding heparin to the solution (final concentration 3.8 μM) and mixing with a pipette prior to fluorescence measurement. The kinetics of aggregation was monitored by fluorescence time scan. Two kinds of buffers were used (a) 50 mM Tris-HCl (pH 7.6), (b) 50 mM MES (pH 6.2).

buffer conditions are altered. On the other hand, CD measurement requires a relatively low concentration of protein ($\sim 2 \mu\text{M}$) and also a buffer other than Tris-HCl, because Cl^- ions affect the far-UV CD spectrum. Therefore, in the CD experiments, a two-step procedure was adopted. In the first step, 4RMBD was incubated to form filaments in Tris-HCl buffer as described in the above section. Then, the sample solution was diluted to 2 μM concentration in 20 mM phosphate buffer (pH 6.8), which is suitable for CD measurement.

Figure 5 demonstrates how the CD spectrum changes as the aggregation reaction proceeds. Each spectrum was recorded at a different time after the aggregation reaction was induced by heparin. In the spectrum of state **S** (time zero), there is a negative peak at 200 nm, indicative of a largely random coil structure (18). Two variations in the CD spectrum should be noted. (i) The intensity of the negative peak at 200 nm decreases as aggregation proceeds. Since this decrease correlates well with the increase in fluorescence intensity in Fig. 4a, we believe that the aggregation of 4RMBD (state **S**) is accompanied by a conformation change. (ii) Accompanying filament formation, a shallow, broad, negative peak appears in the range of 210 nm to 220 nm in the CD spectrum. This may reflect the formation of a local secondary structure. For example, it may be possible that the peptide chains change their folding pattern from a random coil to an aggregated form in the progress of aggregation. Although it is not yet clear which type of secondary structure the

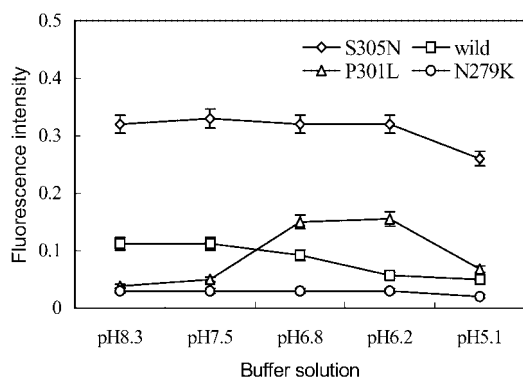


Fig. 7. Effect of pH on the aggregation of different 4RMBD mutants. Five kinds of buffer solutions were used for the aggregation reaction. (i) 50 mM NaAc-HAc (pH 5.1) (ii) 50 mM MES (pH 6.2) (iii) 50 mM PIPES (pH 6.8) (iv) 50 mM Tris-HCl (pH 7.5) (v) 50 mM Tris-HCl (pH 8.3). The concentrations of the wild-type 4RMBD protein and its three mutants were adjusted to 15 μ M using the different buffers containing 1 mM DTT and 10 μ M ThS dye. Aggregation was induced by adding heparin to the solution (final concentration 3.8 μ M) and mixing with a pipette. After incubation for 30 min at 37°C, the fluorescence intensity was measured on a JASCO FP-770F instrument.

aggregated form actually takes, α -helix or β -sheet, the extent of disorder in the overall structure gradually decreases as the filament is formed.

Mutant-dependent Aggregation Rate and pH Effect—It is generally believed that a mutation in the microtubule binding domain plays an important role in PHF formation in frontotemporal dementias FTDP-17 (15–18). Our results indeed support this assumption. The aggregation kinetics of wild-type and mutant 4RMBDs were analyzed by real-time ThS fluorescence assay (Fig. 6). The aggregation rates differ widely among the wild type and mutants. The aggregation of the S305N mutant is exceptionally fast, with a half-time of only 3 min. In contrast, that of the N279K mutant is the slowest, even slower than the wild-type 4RMBD. A previous study revealed that aggregation can be strongly enhanced by point mutations, particularly by the mutation P301L (14). However, the present experiment shows that S305N has a pronounced effect on the aggregation reaction, even larger than that of P301L.

It has been reported that tau aggregation occurs over a wide pH range from 6 to 11, and is most favorable at physiological pH (22). Although filament formation depends on protein-protein or protein-polyanion interactions, any change in pH could affect the charge state of the peptide chain, and thus exert a "perturbation" on the folding shape of the peptide chain. Because different mutants probably have different folding shapes (and thus different aggregation behaviors), we paid attention to another aspect, *i.e.*, how pH affects the aggregation of 4RMBD mutants. The aggregation of the wild-type and three mutant 4RMBDs in five different buffer solutions (pH 8.3–5.1) was investigated by the ThS fluorescence assay. All conditions were the same except for the buffer solution. The results are shown in Fig. 7. Although the maximum fluorescence intensity (an indication of the extent of aggregation) varied with the pH of the buffer solution, the patterns of variation could be divided into

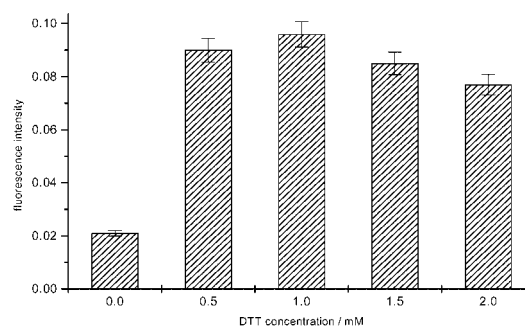


Fig. 8. The effect of DTT on the aggregation of 4RMBD constructs. The concentration of the wild-type 4RMBD protein was adjusted to 15 μ M using 50 mM Tris-HCl (pH 7.5) buffer containing 10 μ M ThS dye and different concentrations of DTT (from 0 mM to 2.0 mM). Aggregation was induced by adding heparin to the solution (final concentration 3.8 μ M) and mixing with a pipette. After incubation for 30 min at 37°C, the fluorescence intensity was measured on a JASCO FP-770F instrument.

three types. The first type is shown by the N279K and S305N mutants. For these mutants, the maximum fluorescence intensity is almost the same in different pH buffers. In other words, the extent of aggregation is little affected by buffer pH. Wild-type 4RMBD shows the second type of pattern. Its aggregation increases with increasing buffer pH. The P301L mutant shows the third type of pattern, with an optimal aggregation rate within pH 6–8. In Tris-HCl buffer, pH 7.5, wild-type 4RMBD aggregates faster than the P301L mutant. A reverse result was observed in MES buffer, pH 6.2. In conclusion, this experiment reveals that pH exerts different effects on aggregation depending on the type of 4RMBD mutant, and tau is at high risk of forming filaments at physiological pH, similar to the case at non-physiological pH, even if tau is in a soluble form.

Effect of DTT on Filament Formation—Wild-type 4RMBD (15 μ M) was mixed with heparin (3.8 μ M) in Tris-HCl buffer (pH 7.5) containing different concentrations of DTT. After incubation for 40 min at 37°C, the fluorescence intensity was measured. Figure 8 illustrates the relationship between fluorescence intensity and DTT concentration. As reflected by the fluorescence intensity, the extent of aggregation was dependent on DTT concentration. Without DTT, the fluorescence intensity was very low. By adding a small amount of DTT to the solution (0.5 mM), the fluorescence intensity increased abruptly, indicating that DTT enhances the aggregation of wild-type 4RMBD. At 1 mM DTT, the fluorescence intensity reached a maximum value. Similar variations were also observed for the mutants. These findings indicate that DTT is helpful for the aggregation reaction. A weakly reductive environment of 1.0 mM DTT is the optimum condition for PHF formation.

DISCUSSION

To examine the mechanism of tau filament formation, recombinant His-tagged 4RMBD constructs were expressed and purified. Although the experiments were performed with the tau constructs, not full-length tau, it was proved that the microtubule binding domain (MBD)

is the most important fragment for microtubule-association, as well as the PHF formation. We believe that our results on 4RMBD aggregation provide useful information for a better understanding of PHF formation in AD brain. The selection of His-tagged 4RMBD is primarily due to its high level of expression and easy purification. By applying cation exchange and gel filtration FPLC, together with a nickel chelating Sepharose column, samples of high purity were conveniently obtained. Although we can not rule out the possibility that the His-tag may exert some influence on aggregation, one important purpose of our present work was to inspect the effects of point mutations. All 4RMBD mutants had the same His-tag, but showed different aggregation behaviors as found by the ThS fluorescence method. We believe that these effects do not result solely from the His-tag. Using gel filtration chromatography and dynamic light scattering, we found that the hydrodynamic radii of 4RMBDs in Tris-HCl buffer were much larger than that anticipated for a 14.5 kDa protein, indicating that 4RMBD normally exists as an oligomer (subunit **S**) in these conditions. By spectroscopic methods, we investigated the aggregation behavior of 4RMBDs from this oligomer state **S**. Several conclusions can be drawn from this research.

(1) *Possible Oligomer State of 4RMBD in Buffer Solution*—Both gel filtration and DLS experiment yield the result that the hydrodynamic radii of 4RMBD constructs are around 3.10 nm (apparent MW corresponding to 45 kDa). However, the non-spherical random structure of 4RMBD makes it difficult to estimate the oligomeric state directly from its hydrodynamic radius (apparent MW). We believe the best way to solve this problem is to compare the hydrodynamic radius with that of a known tau oligomer whose molecular mass is close to that of 4RMBD. Previously, it was reported by Wille *et al.* (24) that the Stokes radius of the K12 construct (13.1 kDa) (Fig. 1) is about 2.5 nm for the monomer and 3.0 nm for the dimer, based on gel filtration chromatography. Compared with 4RMBD, K12 does not have the second repeat in the repeat domain. However, the electron microscopy experiment proved that the length of the repeat domain is approximately independent of the second repeat, and the C-terminal tail is little affected (24). These facts suggest that both 4RMBD and K12 can be considered to have similar rod-like molecular structures of approximately the same length. Therefore, we conclude that subunit **S** with a Stokes radius of 3.1 nm is the dimer of 4RMBD.

It is well known that DTT prevents the formation of disulfide bonds. Heat shock at 50°C for 5 min induces the complete reduction of the tau dimer to the monomer in buffer containing 1–10 mM DTT, provided that the dimer is linked by an intermolecular disulfide bond (14). However, our gel filtration chromatography and DLS showed that the Stokes radii of 4RMBDs did not change when 5 mM DTT was added into the buffer. Moreover, the ThS fluorescence assay also revealed no significant difference in aggregation behavior when the 4RMBDs were heated at 50°C for 10 min in Tris-HCl buffer containing 5 mM DTT prior to the addition of heparin. Because DTT had no effect on oligomerization, we believe that the 4RMBD dimer is formed by non-covalent intermolecular interactions, such as hydrogen bonds, electrostatic and hydro-

phobic interactions, and is not linked by an intermolecular disulfide bond as has been reported for the K19 construct (Fig. 1) (22).

(2) *Could the 4RMBD Non-covalent Dimer Be the Effective Structural Unit for Filament Formation?*—It is widely accepted that the tau dimer is the building block of filaments (20, 25–27). Is it possible that this non-covalent dimer can also be an effective building block for aggregation? Our results appear to give a positive answer. It has been reported that the tau construct containing the four-repeat domain, named K18, assembles into PHF from its monomer state in PBS buffer with a half-life of around 5.5 h (14). In contrast, the present results indicate that 4RMBDs assemble into PHF from the non-covalent dimer state in Tris-HCl buffer with a half-life less than 10 min, much shorter than that of the K18 monomer. Hence it is conceivable that the 4RMBD non-covalent dimer is an effective building block for filament formation. The large difference in aggregation speed between 4RMBD and K18 appears to be due in part to the different buffer conditions, although the effect of the His-tag can not be ignored for 4RMBD.

Friedhoff *et al.* proposed a model for the mechanism of filament formation of tau, in which they believed that the tau dimer linked by an intermolecular disulfide bond is the building block of PHFs, because the oxidation of the SH group promotes the aggregation of tau constructs (19). This is true for a tau construct containing only one SH group in the repeat domain. But for 4RMBD with two SH groups in the repeat domain, a different mechanism should be considered. Under the present situation, the "driving force" of filament formation involves two aspects, i.e., the covalent force caused by the formation of an intermolecular disulfide bond, and the non-covalent force, such as hydrogen bond, electrostatic interaction and/or hydrophobic interaction, resulting from all the intermolecular interactions other than covalent bond. Any structural and/or conformational change to enhance the "driving force" should promote the assembly of tau molecules.

(3) *Conformational Change Is the Prerequisite for Filament Formation*—The CD spectra indicate that a conformational change occurs in the process of filament formation: from a largely random coil conformation to some degree of α -helix and/or β -sheet conformation, although the conformations of α -helix and/or β -sheet could not be definitely characterized due to sensitivity limitations. This result supports the conclusion that PHFs comprise ~85% α -helices, as recently reported by Sadqi *et al.* (25). Moreover, this result hints that a conformational change is a prerequisite for filament formation. The interaction between tau and polyanion is regarded to be the central event in the development of neuropathology in the AD brain (28). Under normal situations, tau is a highly soluble and hydrophilic protein that assumes a largely random coil conformation. However, in the presence of polyanions such as heparin, a coil-helix conformational transition could be induced by the negative charge on the polyanion (29–31). The local secondary structure of α -helix and/or β -sheet formed on the tau peptide chain would activate aggregation through electrostatic and/or hydrophobic interactions (32).

(4) *The S305N Mutant Has the Most Pronounced Effect on Molecular Aggregation*—It is remarkable that the 4RMBD S305N mutant aggregates at an abnormally high rate. This mutation shows the most pronounced effect on filament formation reported so far. This extraordinary enhancement of aggregation is consistent with the observation that the S305N missense mutation of the tau gene is linked to familial tauopathy (33). The present *in vitro* data provide a biochemical understanding for this distinct familial presenile dementia.

Although 4RMBD is necessary for the assembly of tau in Alzheimer paired helical filaments, its core part is the third repeat of MBD (R3, Fig. 1). Electron microscopic analyses showed that the speed of filament formation is on an order of $R3 \gg R2 > R4 = R1$ (16). Therefore, it seems reasonable that the S305N mutant, which is located at the joint position between R2 and R3 repeats, has the most significant effect on the aggregation of 4RMBD. On the other hand, the N279K mutant showed little aggregation despite pH variations. This means that the mutation in FTDP-17 does not inevitably lead to the acceleration of self-aggregation. However, the pathogenic mechanisms of the mutations are potentially multiple, *i.e.*, (i) effects at the RNA level, (ii) a reduction of the ability of tau to interact with microtubules, and (iii) the stimulation of self-assembly. Although we found that N279K aggregates even more slowly than the wild type, N279K may have additional effects, for example, recently we found by the surface plasmon resonance (SPR) method, that the heterogeneous interaction of N279K with the wild type is even stronger than the homogeneous interaction of wild type. In addition, the factor of an inducer molecule should also be taken into consideration. The slower aggregation of N279K may depend on the inducer (in this work, we used heparin as the inducer). So we believe that even the N279K mutation has a negative effect on *in vitro* aggregation, it should not be excluded from the mutations of pathogenic.

(5) *Aggregation of 4RMBDs Is Optimal under a Weakly Reducing Environment*—Which environment, oxidizing or reducing, promotes filament formation? The answer remains controversial. Schweers *et al.* (20) reported that the tau construct K19 possessing three internal repeats (Fig. 1) cannot aggregate effectively in a reductive environment. Wilson and Binder (34), in contrast, found that the tau dimer formed under a less reductive environment inhibits the polymerization process. Our results support the latter conclusion. We found that a weakly reducing environment promotes the aggregation of 4RMBD.

One explanation can be given from the viewpoint of disulfide bond. Because of its reducing properties, DTT usually inhibits the formation of disulfide bonds, and, accordingly, has a negative effect on filament formation, provided that the tau dimer is the effective building block of the filament and a cross-linkage through the Cys residues by a intermolecular disulfide bond is the key structure in the dimer. For K19 (3RMBD), the situation is exactly like this (35). Nevertheless, for tau constructs such as 4RMBD, there are two cysteine residues in the peptide chain (one in R2 and the other in R3, Fig. 1), so both inter-molecular and intra-molecular disulfide bonds are possible. However, under normal conditions (oxidizing or non-reducing environment), intra-molecular

disulfide bonds predominate (entropy priority). Intra-molecular disulfide bond causes the backbone of 4RMBD to be folded, and, thus, is disadvantageous (or even fatal) to tau aggregation. Therefore, 4RMBD can not effectively assemble under this condition. By adding DTT into the solution, intra-molecular disulfide bonds are broken, and the folding shapes of the molecules change to a state favorable for aggregation. So it is conceivable that a small amount of DTT has a positive effect on the aggregation of 4RMBD. On the other hand, because DTT may inevitably block the formation of inter-molecular disulfide bond, higher concentration of DTT may also inhibit the aggregation of 4RMBD, and the extent of aggregation will gradually decrease with increasing DTT concentration. Therefore, it is easy to understand why a weakly reducing environment (1 mM DTT) is optimal for the aggregation of 4RMBD.

The relationship between the reductive state and cell degeneration in AD has drawn increasing attention (36, 37). Our experiments revealed that an oxidizing environment does not invariably promote filament formation. This also implies that reducing reagents should not always be viewed as antidotes for PHF assembly.

This work was supported by Grants-in-Aid for Scientific Research from the Ministry of Education, Culture, Sports, Science and Technology of Japan, by a JSPS Postdoctoral Fellowship for Foreign Researchers (T.-M.Y.), and by The Science Research Promotion Fund of The Promotion and Mutual Aid Corporation for Private Schools of Japan.

REFERENCES

1. Johnson, G.V. and Hartigan, J.A. (1999) Related tau protein in normal and Alzheimer's disease brain. *J. Alzheimers Dis.* **4-5**, 329–351
2. Drewes, G., Trinczek, B., Illenberger, S., Biernat J., Schmitt-Ulms, G., Meyer, H.E., Mandelkow, E.M., and Mandelkow, E. (1995) Microtubule-associated protein/microtubule affinity-regulating kinase (p110mark). A novel protein kinase that regulates tau-microtubule interactions and dynamic instability by phosphorylation at the Alzheimer-specific site serine 262. *J. Biol. Chem.* **270**, 7679–7688
3. Braak, H. and Braak, E. (1997) Frequency of stages of Alzheimer-related lesions in different age categories. *Neurobiol. Aging* **18**, 351–357
4. Goedert, M. and Spillantini, M.G. (2000) Tau mutations in frontotemporal dementia FTDP-17 and their relevance for Alzheimer's disease. *Biochim. Biophys Acta* **1502**, 110–121
5. Foster, N.L., Wilhelmsen, K., Sima, A.A., Jones, M.Z., D'Amato, C.J., and Gilman, S. (1997) Frontotemporal dementia and parkinsonism linked to chromosome 17: a consensus conference. Conference Participants. *Ann. Neurol.* **41**, 706–715
6. Taniguchi, T., Kawamata, T., Mukai, H., Hasegawa, H., Isagawa, T., Yasuda, M., Hashimoto, T., Terashima, A., Nakai, M., Ono, Y., and Tanaka, C. (2001) Phosphorylation of tau is regulated by PKN. *J. Biol. Chem.* **276**, 10025–10031
7. Morishima-Kawashima, M., Hasegawa, M., Takio, K., Suzuki, M., Yoshida, H., Watanabe, A., Titani, K., and Ihara, Y. (1995) Hyperphosphorylation of tau in PHF. *Neurobiol. Aging* **16**, 365–371
8. Sturchler-Pierrat, C., Abramowski, D., Duke, M., Wiederhold, K.H., Mistl, C., Rothacher, S., Ledermann, B., Burki, K., Frey, P., Paganetti, P.A., Waridel, C., Calhoun, M.E., Jucker, M., Probst, A., Staufenbiel, M., and Sommer B. (1997) Two amyloid precursor protein transgenic mouse models with Alzheimer disease-like pathology. *Proc. Natl Acad. Sci. USA* **94**, 13287–13292

9. Wille, H., Drewes, G., Biernat, J., Mandelkow, E.M., and Mandelkow, E. (1992) Alzheimer-like paired helical filaments and antiparallel dimers formed from microtubule-associated protein tau *in vitro*. *J. Cell Biol.* **118**, 573–584
10. Schweer, O., Schonbrunn-Hanebeck, E., Marx, A., and Mandelkow, E. (1994) Structural studies of tau protein and Alzheimer paired helical filaments show no evidence for beta-structure. *J. Biol. Chem.* **269**, 24290–24297
11. Friedhoff, P., Von Bergen, M., Mandelkow, E.M., and Mandelkow, E. (2000) Structure of tau protein and assembly into paired helical filaments. *Biochim. Biophys. Acta* **1502**, 122–132
12. Perez, M., Valpuesta, J.M., Medina, M., Degarcini, E.M., and Avila, J. (1996) Polymerization of tau into filaments in the presence of heparin: the minimal sequence required for tau-tau interaction. *J. Neurochem.* **67**, 1183–1190
13. Hasegawa, M., Crowther, R.A., Jakes, R., and Goedert, M. (1997) Alzheimer-like changes in microtubule-associated protein Tau induced by sulfated glycosaminoglycans. Inhibition of microtubule binding, stimulation of phosphorylation, and filament assembly depend on the degree of sulfation. *J. Biol. Chem.* **272**, 33118–33124
14. Barghorn, S., Zheng-Fischhofer, Q., Ackmann, M., Biernat, J., Von Bergen, M., Mandelkow, E.-M., and Mandelkow, E. (2000) Structure, microtubule interactions, and paired helical filament aggregation by tau mutants of frontotemporal dementias. *Biochemistry* **39**, 11714–11721
15. Foster, N.L., Wilhelmsen, K., Sima, A.A., Joes, M.Z., D'Amato, C.J., and Gilman, S. (1997) Frontotemporal dementia and parkinsonism linked to chromosome 17: a consensus conference. Conference Participants. *Ann. Neurol.* **41**, 706–715
16. Arrasate, M., Perez, M., Armas-Portela, R., and Avila, J. (1999) Polymerization of tau peptides into fibrillar structures. The effect of FTDP-17 mutations. *FEBS Lett.* **446**, 199–202
17. Goedert, M., Jakes, R., and Crowther, R.A. (1999) Effects of frontotemporal dementia FTDP-17 mutations on heparin-induced assembly of tau filaments. *FEBS Lett.* **450**, 306–311
18. Von Bergen, M., Barghorn, S., Li, L., Marx, A., Biernat, J., Mandelkow, E.M., and Mandelkow, E. (2001) Mutations of tau protein in frontotemporal dementia promote aggregation of paired helical filaments by enhancing local beta-structure. *J. Biol. Chem.* **276**, 48165–48174
19. Friedhoff, P., Von Bergen, M., Mandelkow, E.M., Davies, P., and Mandelkow, E. (1998) A nucleated assembly mechanism of Alzheimer paired helical filaments. *Proc. Natl Acad. Sci. USA* **95**, 15712–15717
20. Schweers, O., Mandelkow, E.M., Biernat, J., and Mandelkow, E. (1995) Oxidation of cysteine-322 in the repeat domain of microtubule-associated protein tau controls the *in vitro* assembly of paired helical filaments. *Proc. Natl Acad. Sci. USA* **92**, 8463–8467
21. Roher, A., Palmer, K., Chau, V., and Ball, M. (1988) Isolation and chemical characterization of Alzheimer's disease paired helical filament cytoskeletons: differentiation from amyloid plaque core protein. *J. Cell Biol.* **107**, 2703–2716
22. Friedhoff, P., Schneider, A.E.M., Davies, P., and Mandelkow, E. (1998) Rapid assembly of Alzheimer-like paired helical filaments from microtubule-associated protein tau monitored by fluorescence in solution. *Biochemistry* **37**, 10223–10230
23. Kelly, S.M. and Price, N.C. (1997) The application of circular dichroism to studies of protein folding and unfolding. *Biochim. Biophys. Acta* **1338**, 161–185
24. Wille, H., Drewes, G., Biernat, J., Mandelkow, E.M., Mandelkow, E., (1992) Alzheimer-like paired helical filaments and antiparallel dimers formed from microtubule-associated protein tau *in vitro*. *J. Cell Biol.* **118**, 573–584
25. Sadqi, M., Hernandez, F., Pan, U., Perez, M., Schaeberle, M.D., Avila, J., Munoz V. (2002) Alpha-helix structure in Alzheimer's disease aggregates of tau-protein. *Biochemistry* **41**, 7150–7155
26. Von Bergen, M., Friedhoff, P., Biernat, J., Heberle, J., Mandelkow, E.M., and Mandelkow, E. (2000) Assembly of tau protein into Alzheimer paired helical filaments depends on a local sequence motif [(306)VQIVYK(311)] forming beta structure. *Proc. Natl Acad. Sci. USA* **97**, 5129–5134
27. Bhattacharya, K., Rank, K.B., Evans, D.B., and Sharma, S.K. (2001) Role of cysteine-291 and cysteine-322 in the polymerization of human tau into Alzheimer-like filaments. *Biochem. Biophys. Res. Commun.* **285**, 20–26
28. Goedert, M., Jakes, R., Spillantini, M.G., Hasegawa, M., Smith, M.J., and Crowther, R.A. (1996) Assembly of microtubule-associated protein tau into Alzheimer-like filaments induced by sulphated glycosaminoglycans. *Nature* **383**, 550–553
29. Paudel, H.K. and Li, W. (1999) Heparin-induced conformational change in microtubule-associated protein Tau as detected by chemical cross-linking and phosphopeptide mapping. *J. Biol. Chem.* **274**, 8029–8038
30. Takahashi, Y., Ueno, A., and Mihara, H., (1999) Optimization of hydrophobic domains in peptides that undergo transformation from alpha-helix to beta-fibril. *Bioorg. Med. Chem.* **7**, 177–185
31. Bieri, O. and Kiefhaber, T. (1999) Elementary steps in protein folding. *Biol. Chem.* **380**, 923–929
32. Minoura, K., Tomoo, K., Ishida, T., Hasegawa, H., Sasaki, M., and Taniguchi, T. (2002) Amphipathic helical behavior of the third repeat fragment in the tau microtubule-binding domain, studied by ¹H NMR spectroscopy. *Biochem. Biophys. Res. Commun.* **294**, 210–214
33. Iijima, M., Tabira, T., Poorkaj, P., Schellenberg, G.D., Trojanowski, J.Q., Lee, V.M., Schmidt, M.L., Takahashi, K., Nabika, T., Matsumoto, T., Yamashita, Y., Yoshioka, S., and Ishino, H. (1999) A distinct familial presenile dementia with a novel missense mutation in the tau gene. *Neuroreport* **10**, 497–501
34. Wilson, D.M. and Binder, L.I. (1995) Polymerization of microtubule-associated protein tau under near-physiological conditions. *J. Biol. Chem.* **270**, 24306–24314
35. Kampers, T., Friedhoff, P., Biernat, J., Mandelkow, E.M., and Mandelkow, E. (1996) RNA stimulates aggregation of microtubule-associated protein tau into Alzheimer-like paired helical filaments. *FEBS Lett.* **399**, 344–349
36. Smith, C.D., Carney, J.M., Starke-Reed, P.E., Oliver, C.N., Stadtman, E.R., Floyd, R.A., and Markesbery, W.R. (1991) Excess brain protein oxidation and enzyme dysfunction in normal aging and in Alzheimer disease. *Proc. Natl Acad. Sci. USA* **88**, 10540–10543
37. Behl, C., Davis, J.B., Lesly, R., and Schubert, D., (1994) Hydrogen peroxide mediates amyloid beta protein toxicity. *Cell* **77**, 817–827